# Oscillation annealing in Electronic Power Steering (EPS) systems

Valentina Ciarla, Carlos Canudas de Wit, Franck Quaine, Violaine Cahouet

# Oscillation annealing in Electronic Power Steering (EPS) systems

V. Ciarla, C. Canudas de Wit, F. Quaine, V. Cahouet

*Laboratoire d'Automatique de Grenoble GIPSA-Lab, UMR 5216, France*

## *Abstract*

This document is a working report concerning the Task 5.1 of the project **VolHand 09 VTT 14** and refers to the paper [1]. This task is competence of the GipsaLab.
This report presents several aspects of modelling, observation and control towards a new generation of Electrical Power Steering(EPS) systems. In particular authors design an optimal control to reject oscillations of the steering column. Authors also revisited the LuGre tire dynamic friction model by improving the transient behaviour between the sticking phases and the dynamic ones. Simulation of the proposed control are shown at the end of the document.

# Contents

# 1 Introduction

According to the document **ANR 09 VTT VOLHAND Doc B**, presented on **October 2011**, the research team in Gipsa-Lab is involved into the task 5.1 (T5.1) for the design of the control law to eliminate the high frequency oscillations of the steering column. To attempt to this job, the following steps have been done:

1. The study of a mechanical model of the Electronic Power Steering (EPS) system and design of an LQR regulator to reject the typical oscillations, due to the torsion of the steering wheel (Paragraph 2)
2. The design of an estimation of the full set of state variables as well as of the exogenous torques is carried out.
3. Modelling of the tyre/road contact friction, in order to test the mathematical model uder the most realistic conditions (Paragraph 3).
4. Study of the amplification curves, in order to provide the correct steering assistance to the driver.

The general architecture that authors propose to study the EPS system is shown in Figure 1. This report concerns the block 1 (observer/control), and the block 2 (tire-friction model) of Figure 1, with the additional contribution that the observer also estimate the driver's and load torque. The design of the specific reference model (block 3) is under current investigation (tasks 5.2 - 5.3 and 5.4).

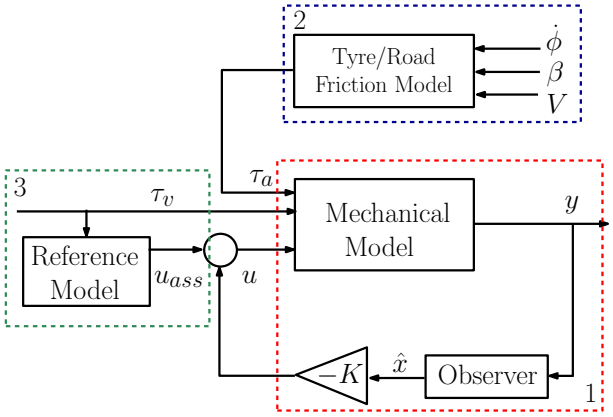


Figure 1: General architecture of the EPS system: block 1 concerns the observer and the control; block 2 includes the tyre-friction model and block 3 includes the reference model.

# 2 Oscillation annealing

## 2.1 Column model

To begin with, it is essential to define the mechanical system to study. Figure 2 shows an explanatory schema of the system. From left to right, it is possible to find:

- the driver's exerted torque, $\tau_v$, as an exogenous input;
- the steering wheel, represented as an inertia $J_v$ with a given local viscosity $B_v$;
- the stiffness of the steering column represented by the coefficient $k$;

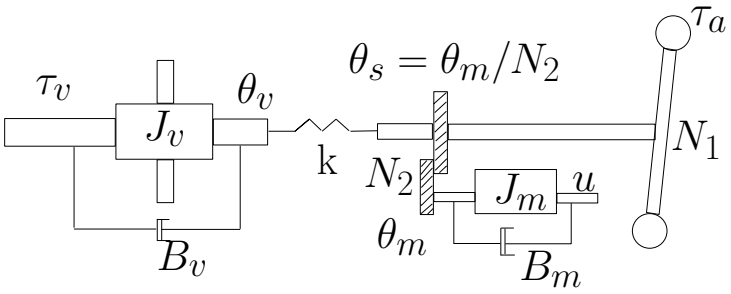


Figure 2: Mechanical model of the EPSs

- the assistance motor, similarly to the steering wheel, modelled as an inertia $J_m$ and a local damping $B_m$;
- gear ratio $N_2$ that connects the assistance motor to the steering column;
- gear ratio $N_1$ that connects the the steering column to the wheels;
- the control inputs $u$ and the exogenous input $\tau_a$, given by the road/tyre friction torque.

The mechanical equations governing the system explained above are inspired from [2] and describe the system as follows:

$$J_v\ddot{\theta}_v = \tau_v - k(\theta_v - \theta_s) - B_v\dot{\theta}_v \quad (1)$$

$$J_T\ddot{\theta}_s = -k(\theta_s - \theta_v) - N_2^2 B_m\dot{\theta}_s + \frac{\tau_a}{N_1} + N_2 u \quad (2)$$

with $J_T = \left(J_c + N_2^2 J_m + \frac{J_w}{N_1^2}\right)$. The constants of the model are reported in Table 1, while $\theta_m$ is the motor angle $[rad]$, $\theta_v$ is the steering wheel angle $[rad]$ and $\theta_s$ is the driving shaft angle after the gear ratio, i.e.:

$$\theta_s = \frac{\theta_m}{N_2} \quad (3)$$

## 2.2 State-space representation

Being the first objective to compensate the oscillations due to the torsion force $F_t = k(\theta_v - \theta_s)$ of the steering wheel, the synthesis of an optimal Linear Quadratic Regulator (LQR) controller is

| Symbol | Description | Value |
|---|---|---|
| $J_v$ | Steering wheel inertia | 0.025 $\mathrm{kgm}^2$ |
| $J_m$ | Motor inertia | 0.0004 $\mathrm{kgm}^2$ |
| $J_c$ | Column inertia | 0.04 $\mathrm{kgm}^2$ |
| $J_w$ | Rack inertia | 0.000784 $\mathrm{kgm}^2$ |
| $k$ | Column stiffness | 100 $\mathrm{N\,m\,rad}^{-1}$ |
| $N_1$ | Steering column-wheels gear ratio | 13.67 |
| $N_2$ | Motor-steering column gear ratio | 17 |
| $B_v$ | Steering wheel viscosity | 0.01 $\mathrm{N\,m\,rad}^{-1}\,\mathrm{s}^{-1}$ |
| $B_m$ | Motor shaft viscosity | 0.0032 $\mathrm{N\,m\,rad}^{-1}\,\mathrm{s}^{-1}$ |

Table 1: Constant parameters of the EPSs

proposed. At this purpose, it is necessary to use a state-space representation of the system. The following choice of the state variables is made:

$$x = \begin{pmatrix} x_1 \\ x_2 \\ x_3 \end{pmatrix} = \begin{pmatrix} \dot{\theta}_v \\ \dot{\theta}_s \\ \theta_v - \theta_s \end{pmatrix} \tag{4}$$

The model can be formulated into the following state-space form:

$$\dot{x} = Ax + Bu + Gw \tag{5}$$

with the disturbances vector $w^T = \left(\tau_v, \tau_a\right)^T$ and following state matrices

$$A = \begin{pmatrix} -\frac{B_v}{J_v} & 0 & -\frac{k}{J_v} \\ 0 & -\frac{N_2^2 B_m}{J_T} & \frac{k}{J_T} \\ 1 & -1 & 0 \end{pmatrix} \tag{6}$$

$$B = \begin{pmatrix} 0 \\ \frac{N_2}{J_T} \\ 0 \end{pmatrix} \tag{7}$$

$$G = \begin{pmatrix} \frac{1}{J_v} & 0 \\ 0 & \frac{1}{N_1 J_T} \\ 0 & 0 \end{pmatrix} = \begin{pmatrix} g_1 & g_2 \end{pmatrix} \tag{8}$$

## 2.3 Open loop model

Once the space state representation of the mechanical model has been completely defined, the interest is to observe how the model responds to a variation of the torque exerted by the driver on the steering wheel. For that to be done, authors compute the transfer function of the steering wheel's angular velocity $\dot{\theta}_v$ in relation to the driver's exerted torque $\tau_v$. Such transfer function is easily calculated from the state-space matrices as follows:

$$G_{ol} = \frac{\dot{\theta}_v}{\tau_v} = C(sI - A)^{-1} G_1 \tag{9}$$

where $C = \left(1, 0, 0\right)$ is the output vector.
The frequency response of the open loop system, described in Eq. (9), is shown in Figure 3. The system has a significant peak for a frequency of about 12 Hz, that might cause important oscillations on the steering wheel. The goal of the control design is to compensate these oscillations, on order to improve the driver's comfort and safety.

## 2.4 Optimal control based on full state-feedback

To compensate the oscillations that might appear in the steering wheel, an optimal LQR controller is implemented. This controller is calculated so that the state-feedback law $u = -Kx$ (with K the state-feedback gain) minimizes a cost function given by the expression:

$$J(x,u) = \int_0^\infty (x^T Q x + u^T R u)\, \mathrm{d}t \tag{10}$$

where the constant matrices $Q$ and $R$ are chosen in order to penalize, respectively, the states and the control inputs in the cost function. To solve this optimization problem it is necessary to solve the following algebraic Riccati equation:

$$A^T P + PA - PBR^{-1}B^T P + Q = 0 \tag{11}$$

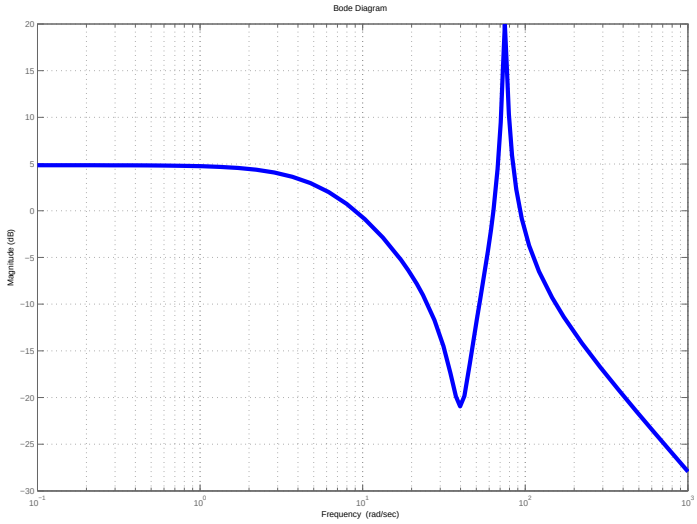


Figure 3: Frequency response of the transfer function $G_{ol}$ in Eq. (9)

whose solution $P$ is used to calculate the state-feedback gain: $K = R^{-1}B^T P$. To synthesize this controller the first step to do is to select the adequate penalization matrices for our specific problem. Three possible choices are encountered:

1. penalization on the variation of the torsion and the torsion rate;
2. penalization on the torsion rate;
3. penalization on the torsion.

### 2.4.1 Penalization on the variation of the torsion and the torsion rate

In this case, the cost function to minimize has the form:

$$J(x,u) = \int_0^\infty (q_1(x_1 - x_2)^2 + q_2 x_3^2 + Ru)\mathrm{d}t \tag{12}$$

To respect the restriction on the matrix $Q$ (it has to be positive or semi-definite positive and symmetric) an easy way to build it is to take an "output" matrix representing the state variables to penalize. In this case:

$$C_q = \begin{pmatrix} q_1 & -q_1 & 0 \\ 0 & 0 & q_2 \end{pmatrix} \tag{13}$$

and the matrix penalizing the states is computed as follows:

$$Q = C_q^T C_q = \begin{pmatrix} q_1 & -q_1 & 0 \\ -q_1 & q_1 & 0 \\ 0 & 0 & q_2 \end{pmatrix} \tag{14}$$

Thus, the value R of the penalization on the control input is normalized and set to 1. Consequently, the values of the parameters $q_1$ and $q_2$ that define the matrix Q must be sufficiently high, such that the states are correctly penalized in the cost function. The chosen values are, respectively, 3 and 12. Therefore:

$$Q = \begin{pmatrix} 3 & -3 & 0 \\ -3 & 3 & 0 \\ 0 & 0 & 12 \end{pmatrix}; \quad R = 1 \tag{15}$$

Once the state-feedback gain has been calculated, the closed loop transfer function is given by the following equation:

$$G_{cl} = \frac{\dot{\theta}_v}{\tau_v} = C(sI - (A - BK))^{-1} G_1 \tag{16}$$

with $(A - BK)$ the closed-loop state space matrix. To prove the performances of the state-feedback

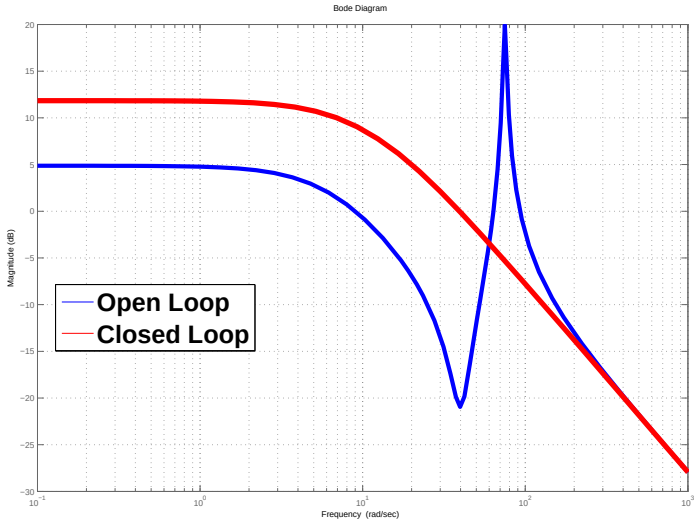


Figure 4: Open loop vs closed loop frequency response

implemented, the closed-loop frequency response is calculated. As it is possible to observe in Figure 4 the resonance peaks that might cause undesirable oscillations have been eliminated thanks to the optimal linear control computed and implemented. However, the gain for low frequencies has been sensibly increased. This fact might affect the performances of the system.

### 2.4.2 Penalization on the variation of the torsion rate

Next, it is also possible to penalize only the torsion rate. This implies to minimize the following cost function:

$$J(x,u) = \int_0^\infty (q_1(x_1 - x_2)^2 + Ru)\mathrm{d}t \tag{17}$$

For this reason, the matrix used to penalize the states in the cost function is:

$$Q = \begin{pmatrix} q_1 & -q_1 & 0 \\ -q_1 & q_1 & 0 \\ 0 & 0 & 0 \end{pmatrix} \tag{18}$$

with $q_1 = 7$ and $R = 1$. It can be observed in Figure 5 that the frequency response in this case is very close to that obtained in the case of penalizing the variation of the torsion and the torsion rate.

### 2.4.3 Penalization on the torsion

Finally, the objective is to penalize only the torsion; that is, to have a cost function of the form:

$$J(x,u) = \int_0^\infty (q_2 x_3^2 + Ru)\mathrm{d}t \tag{19}$$

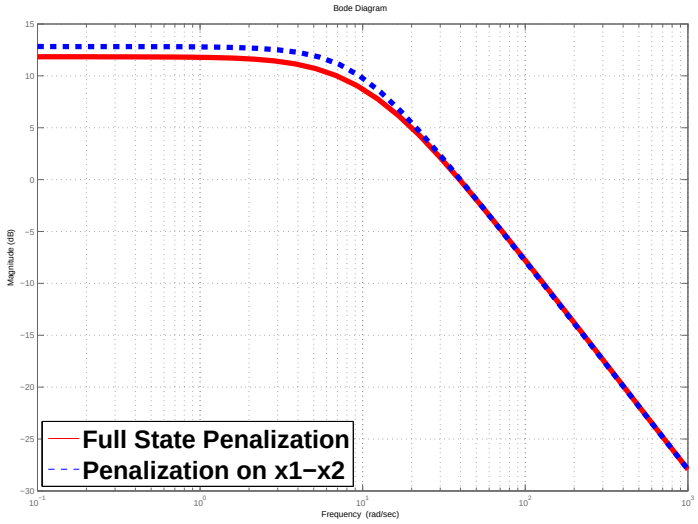


Figure 5: Full state penalization (solid) vs torsion velocity penalization

Thus, following the same reasoning as in the previous cases,

$$C_q = \begin{pmatrix} 0 & 0 & q_2 \end{pmatrix} \tag{20}$$

the corresponding covariance matrix is

$$Q = \begin{pmatrix} 0 & 0 & 0 \\ 0 & 0 & 0 \\ 0 & 0 & q_2 \end{pmatrix} \tag{21}$$

with $q_2 = 200$ and $R = 1$. Figure 6 shows that the fact of only penalizing the torsion affects slightly

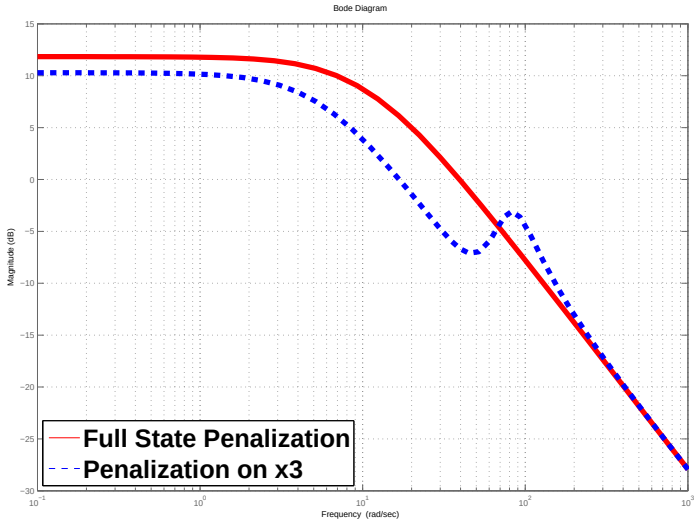


Figure 6: Full state penalization (solid) vs torsion penalization

on the frequency response since there is a small peak where the oscillations occurred for the open loop case. However, the magnitude of such a peak is not at all significant for the performance of the closed-loop system.

## 2.5 Optimal control based on acceleration

To evaluate the performances of the controller in terms of comfort improvement, it is common to consider the transfer function between the steering wheel acceleration $\ddot{\theta}_v$ and the driver's exerted torque. Such a transfer function is calculated from the state-space matrices as follows:

$$G_{ol} = \frac{\ddot{\theta}_v}{\tau_v} = T(sI - A)^{-1}G_1 \tag{22}$$

where $T = \left(-\frac{B_v}{J_v}, 0, -\frac{k}{J_v}\right)$. The corresponding frequency response is shown in Figure 7 the system has a significant peak for a frequency of about 12 Hz that might cause important oscillations on the steering wheel that would rather be avoided so as to improve the driving comfort. In Figure 7, it

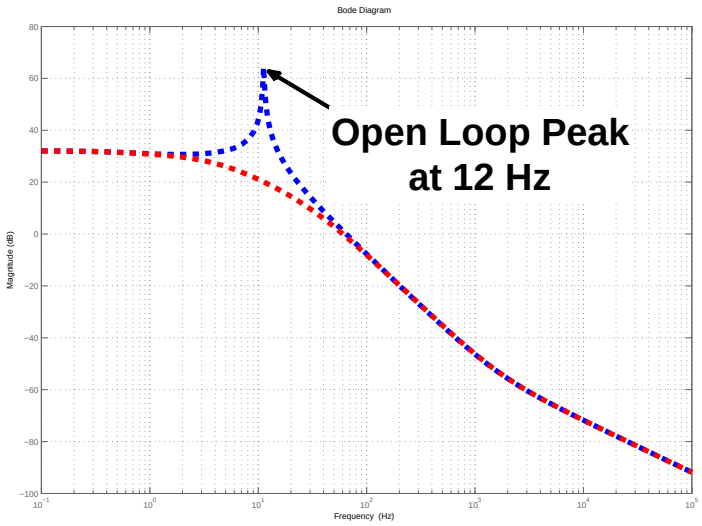


Figure 7: Open loop (blue) vs closed loop frequency response. Weighting parameters are: $q_1 = 3$ and $q_2 = 12$, $r = 1$.

is possible to observe the benefits of the proposed controller. The resonance peak that might cause undesirable oscillations have been eliminated thanks to the proposed optimal linear control. Note also that the low-frequency gain has kept unchanged.

## 2.6 Optimal "output" feedback controller

All the calculations that have been previously carried out assumed that the whole set of state-space variables was measurable, that is, it was possible to obtain exact values of those variables. On the contrary, the actual mechanical model is not provided with sensors to measure all the variables, because of the important extra cost for the installation of these devices.
On a common power steering problem, the variables that are measured are those concerning the assistance motor, either $\theta_s$ or $\dot{\theta}_s$. We assume then $\dot{\theta}_s$ as the output of the system, that is, $\tilde{C} = (0, 1, 0)$. The other state variables are not directly measurable so it is necessary to calculate a state observer to reconstruct the full state so as to implement the full state-feedback computed in previous sections. Being our system $\dot{x} = Ax + Bu + Gw$ the observer will be:

$$\dot{\hat{x}} = (A - L\tilde{C})\hat{x} + Bu + Gw + Ly \tag{23}$$

In Eq. (23), $L$ is the observer gain and is chosen via pole placement method or via the loop recovery strategy. Thus $L$ is chosen so as to have a fast error dynamics and hence a fast convergence of the observer towards the real states.

## 2.7 Simulation results

In order to see the performances of the proposed controller, following simulations are carried out using as input to the system the driver's exerted torque profile shown in Fig. 8-a.

**Open loop behaviour:** the first simulation concerns the system in open loop. As shown at the Figure 8-b, once the steering wheel is released by the driver at the time instant 16 s, the steering wheel suffers significant oscillations that would cause an undesirable driving feeling and might even be dangerous when we are in driving situations at fast speeds.

**Closed-loop behaviour:** the optimal linear controller computed before has the aim to eliminate the oscillations found in open loop thanks to the assistance motor. As shown at the Figure 8-c, the oscillations derived from the release of the steering wheel have been satisfactorily compensated by the optimal controller. The behavior of the observer is shown by Figure 8-d. From this figure we see that the performance of the observer is completely satisfactory.

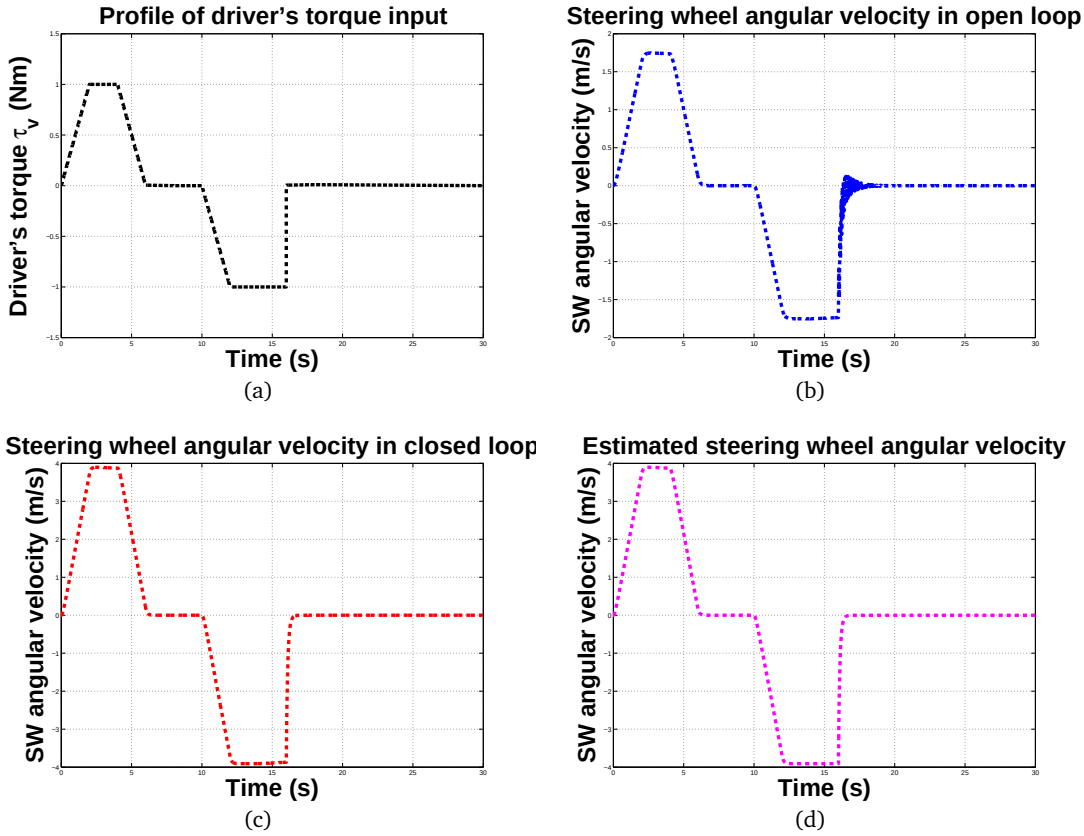


Figure 8: (a) Real driver's steering torque used for the simulation. (b) Profile of the steering wheel speed in open loop. (c) Profile of the steering wheel speed in closed loop. (d) Estimation of the steering wheel speed.

# 3 Road/tyre contact friction torque

The model used until now takes into account all the elements that go from the steering wheel to the steering shaft. Load torques exerted by the tyre/road contact need to be considered explicitly in the model. The contact friction force is an element of the driving that is very important since it is present in all the different driving situations that a driver may find.
To be able to reproduce this contact friction force it is necessary to have a model of the vehicle. However, the fact of developing and implementing a complete vehicle model entails a huge complexity. Thus, and as it is not essential for the development of our simulations, the model chosen is a simplified model of the tyres assuming that the normal force on them is equal to a quarter of the total weight of the vehicle.
Figure 9 shows a tyre as well as both the normal and the lateral velocities ($v_x$ and $v_y$) that might appear when driving. This lateral force that takes part of the model when turning is the reason why the so-called slip angle $\beta$ appears. Thus, the slip angle has to be computed. It depends from

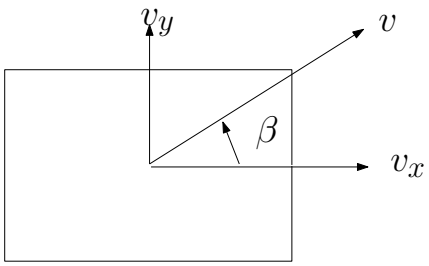


Figure 9: Forces action on the tire when turning. Slip angle $\beta$ show the direction of the vehicle resulting velocity

the speed of the vehicle and the radius of curvature given by the curve traced by the vehicle in a given moment, that is: $\beta(t) = f(v, \rho)$. The radius of curvature can be considered as being inversely proportional to the steering wheel angle: an infinite radius of curvature means the vehicle is going straight and hence the steering wheel angle is zero.
The slip angle is considered to be zero in the cases when the vehicle is stopped or it is not in a cornering situation. Besides, the slip angle is proportional to the speed of the vehicle and the steering wheel angle. Furthermore, the values of the slip angle will not be very high as the situations that will be handled are mainly low speed manoeuvres that would not possibly exceed 30 km/h. Thus, the slip angle does not normally go above 5 $deg$.

## 3.1 Dynamic tyre friction model

The dynamic model used so as to represent the forces and torques caused by the contact of the tyres and the road is an extension to the LuGre dynamic friction model presented in the paper [4]. The objective of this friction model is to capture the different phenomena presents on a real driving situation so as to obtain simulations as trustworthy as possible. The most important phenomena are described below:

- *Self-alignement torque*: it is the torque that appears as the vehicle rolls along that tends to rotate the wheels around its vertical axis in order to make them return to the straight position.
- *Sticking torque*: it is the torque that opposes the movement of the tyres when turning them around the vertical axis. It is especially important for low speeds of the vehicle

The dynamic LuGre Friction model proposed in [4, 5] derives from a distributed friction model. It is described by four differential equations, which capture the average behaviour of the internal friction

states. To introduce this model, let $\bar{z}_i(t)$ $(i = x, y)$, $\hat{z}_y(t)$ denote the internal states of the system:

$$\dot{\bar{z}}_i(t) = v_{ri} - C_{0i}(v_r)\bar{z}_i(t) - \kappa_i^{ss}|\omega r|\bar{z}_i(t) \quad (i = x, y) \tag{24}$$

$$\dot{\hat{z}}_y(t) = \frac{G}{F_n L}v_{ry} - C_{0y}(v_r)\hat{z}_y(t) - v^{ss}|\omega r|\hat{z}_y(t) + \frac{|\omega r|}{L}\bar{z}_y(t) \tag{25}$$

where $v_r = [\ v_{rx} \quad v_{ry}\ ]^T$ is the vector of the relative speeds:

$$v_{rx} = \omega r - v cos(\beta) \tag{26}$$

$$v_{ry} = -v sin(\beta) \tag{27}$$

with $\omega$ that corresponds to the angular velocity of the wheel of radius $r$, while $v$ is the velocity of the vehicle and $\beta$ is the slip angle.
The scalar function $C_{0i}(v_r)$ (with i = x, y) is peculiar of the LuGre model and is given by:

$$C_{0i}(v_r) = \frac{\lambda(v_r)\sigma_{0i}}{\mu_{ki}^2} \tag{28}$$

with

$$\lambda(v_r) = \frac{||M_k^2 v_r||}{g(v_r)} \tag{29}$$

In Eq. (29) it is possible to recognize the the matrix of the kinetic friction coefficients $M_k = \begin{bmatrix} \mu_{kx} & 0 \\ 0 & \mu_{ky} \end{bmatrix} > 0$ for the motion along the $x$ and the $y$ directions, respectively; note also that each parameter $\mu_{ki}$ in Eq. (28) corresponds to one element on the main diagonal of matrix $M_k$. We find also the function $g\left(v_r\right)$, given by:

$$g\left(v_r\right) = \frac{\left\|M_k^2 v_r\right\|}{\left\|M_k v_r\right\|} + \left(\frac{\left\|M_s^2 v_r\right\|}{\left\|M_s v_r\right\|} - \frac{\left\|M_k^2 v_r\right\|}{\left\|M_k v_r\right\|}\right) e^{-\left(\frac{\|v_r\|}{v_s}\right)^\gamma} \tag{30}$$

with $M_s = \begin{bmatrix} \mu_{sx} & 0 \\ 0 & \mu_{sy} \end{bmatrix} > 0$ that is the matrix of static friction coefficients.
To evaluate the constants $\kappa_i^{ss}$ and $v^{ss}$, we do the hypothesis that the steady-state solution of the lumped model is the same with the steady-state solution of the distributed one. The complete expression of these parameters is given from:

$$\kappa_i^{ss} = \frac{1}{|\omega r|}\left(\frac{v_{ri}}{\bar{z}_i^{ss}} - C_{0i}(v_r)\right) \tag{31}$$

$$v^{ss} = \frac{1}{|\omega r|}\left(\frac{1}{\hat{z}_y^{ss}}\left(\frac{G v_{ry}}{F_n L} + \frac{|\omega r|\bar{z}_y^{ss}}{L}\right) - C_{0y}\right) \tag{32}$$

with $\bar{z}_i^{ss}$ and $\hat{z}_y^{ss}$, that are the steady-states of the system; the explicit expression for these parameters is given in the Appendix.
The auto-aligning torque can be written in terms of the mean states $\bar{z}_y(t)$ and $\hat{z}_y(t)$ as follows:

$$M_{self-alig} = F_n L\left[\sigma_{0y}\left(\frac{1}{2}\bar{z}_y(t) - \hat{z}_y(t)\right) + \sigma_{1y}\left(\frac{1}{2}\dot{\bar{z}}_y(t) - \dot{\hat{z}}_y(t)\right) + \sigma_{2y}\left(\frac{1}{2}v_{ry} - \frac{G}{F_n L}\right)\right] \tag{33}$$

To calculate the sticking torque we introduce the last equation of the LuGre model:

$$\dot{z}_z = \dot{\phi} - \frac{\sigma_{0z}|\dot{\phi}|}{g_z(\dot{\phi})}z_z(t) \tag{34}$$

| Symbol | Value | Description |
|---|---|---|
| $r$ | wheel radius | 0.38 m |
| $v$ | vehicle speed | range from 0 to 30 $\mathrm{km\,h^{-1}}$ |
| $\omega$ | angular velocity of the wheel | $\omega = v/r$ $\mathrm{rad\,s^{-1}}$ |
| $\mu_{kx}$ | kinetic friction coeff. x-axis | 0.75 |
| $\mu_{ky}$ | kinetic friction coeff. y-axis | 0.75 |
| $\mu_{kz}$ | kinetic friction coeff. z-axis | 0.76 |
| $\mu_{sx}$ | static friction coeff. x-axis | 1.35 |
| $\mu_{sy}$ | static friction coeff. y-axis | 1.40 |
| $\mu_{sz}$ | static friction coeff. z-axis | 0.91 |
| $v_s$ | Stribeck relative velocity | $3.96\ \mathrm{m\,s^{-1}}$ |
| $\dot{\phi}_s$ | Stribeck relative velocity | $74\ \mathrm{rad\,s^{-1}}$ |
| $\gamma$ | steady state constant | 1 |
| $\sigma_{0y}$ | normalized rubber stiffness | $6000\ \mathrm{N\,m^{-1}}$ |
| $\sigma_{1y}$ | normalized rubber damping | $0.3568\ \mathrm{N\,m^{-1}\,s^{-1}}$ |
| $\sigma_{2y}$ | normalized viscous relative damping | $0.0001\ \mathrm{N\,m^{-1}\,s^{-1}}$ |
| $L$ | patch length | 0.15 m |
| $\zeta_L$ | left patch length | 0.0030 m |
| $\zeta_R$ | right patch length | 0.1155 m |
| $F_{max}$ | max value of normal load distribution | 1900 N |
| $F_n$ | normal value of normal load distribution | 249.37 N |
| $\alpha_1$ | coeff. for Self-Align. torque | $63000\ \mathrm{N\,m^{-1}}$ |
| $\alpha_2$ | coeff. for Self-Align. torque | $-55000\ \mathrm{N\,m^{-1}}$ |
| $\beta_2$ | coeff. for Self-Align. torque | 8260 N |
| $\sigma_{0z}$ | coeff. for Stick. torque | 20 |
| $\sigma_{1z}$ | coeff. for Stick. torque | 0.0023 |
| $\sigma_{2z}$ | coeff. for Stick. torque | 0.0001 |
| $G$ | load distribution function | $16.83\ \mathrm{Nm^2}$ |
| $\kappa_i^{ss}$ | function used to approx. steady behavior | 11.9 |
| $\nu^{ss}$ | function used to approx. steady behavior | $-0.8$ |

Table 2: Constant parameters of the LuGre model

where the angular velocity of the wheel rim is $\dot{\phi} = \dot{\theta}_s/N_1$, and and the function

$$g_z\left(\dot{\phi}\right) = \mu_{kz} + \left(\mu_{sz} - \mu_{kz}\right) e^{-\left(\frac{\dot{\phi}}{\dot{\phi}_s}\right)^2} \tag{35}$$

where $\mu_{kz}$ and $\mu_{sz}$ are, respectively, the kinetic and static friction coefficients across the z-axis, while $\dot{\phi}_s$ is the Stribeck velocity.
The sticking torque can be evaluated as follows:

$$M_{sticking} = -LF_n(\sigma_{0z}z_z(t) + \sigma_{1z}\dot{z}_z(t) + \sigma_{2z}\dot{\phi}) \tag{36}$$

Hence, the total torque generated by the contact of the tyres and the road is:

$$\tau_a = M_{self-alig} + M_{sticking} \tag{37}$$

The parameters used in this model are reported in Table 2.

### 3.2 Friction model improvements

During the analysis of equations of the LuGre model, there are some parameters that are crucial to the behaviour of the sticking torque and can be set in order to improve the realistic behaviour of the model.

### 3.2.1 The approximate torque exerted on the wheels

This parameter $F_n L$ can be chosen experimentally by measuring the necessary torque to be exerted in order to start moving the wheels without assistance when being at a standstill. As by now these measures are not available, it can be assumed that a torque of about 50 Nm appears on the wheels before starting to move. Since the sticking torque is introduced directly on the steering column on the model presented, the motor/steering colon gear ratio has to be taken into account. Hence, $F_n L$ should have an approximate value of $F_t = \frac{50}{N_2}$

### 3.2.2 Coefficients of the sticking torque

This coefficient $\sigma_{0z}$ affects directly on the settling time of the sticking torque. It is important to notice that very fast dynamics make the sticking torque vary in steps. This includes very high frequency components that are likely to cause oscillations and instabilities. Thus, it is advisable to choose a value for $\sigma_{0z}$ low enough so as to avoid too fast dynamics. In this case the value chosen was $\sigma_{0z} = 0.0001$.
The value $\sigma_{1z}$ is chosen conveniently to avoid overshoot in the dynamics of the sticking torque.

### 3.2.3 Dependency on vehicle's speed

One possible improvement of the previous model concerns the the dependence of the sticking torque to the vehicle velocity, $v$. In fact, it can be proved experimentally that, as the speed of the vehicle grows, the self-alignment torque dominates over the sticking torque, and inversely. The previous model in its actual form, does not respect this observation. It is then necessary to weight the sticking torque as a function the velocity of the vehicle. Thus, a possible modification along these observations is:

$$M_{sticking} = -LF_n(\sigma_{0z} z_z + \sigma_{1z}\dot{z}_z + \sigma_{2z}\dot{\phi})e^{-|v|/v_k} \tag{38}$$

where $v_k$ is a positive constant.

## 3.3 Simulation results

It is also important to check if the results follow the expected logic when we vary the vehicle's speed. In order to do this, several simulations were carried out for velocities going from 0 to 30 $\mathrm{km\,h^{-1}}$ and over a range time of several seconds, in order to see the effects at steady-state. The choice of this speed range is due to the fact that an EPSs operate in this range.
The results obtained from those simulations are shown in Figure 10:

- Figure 10(a) shows the different curves obtained for the sticking torque for different driving speeds, while Figure 10(b) shows the different curves obtained for the self-alignment torque. Results are as expected: the sticking torque decreases exponentially as the velocity increases, so as the contribution of the self-alignment is more important as the speed increases.

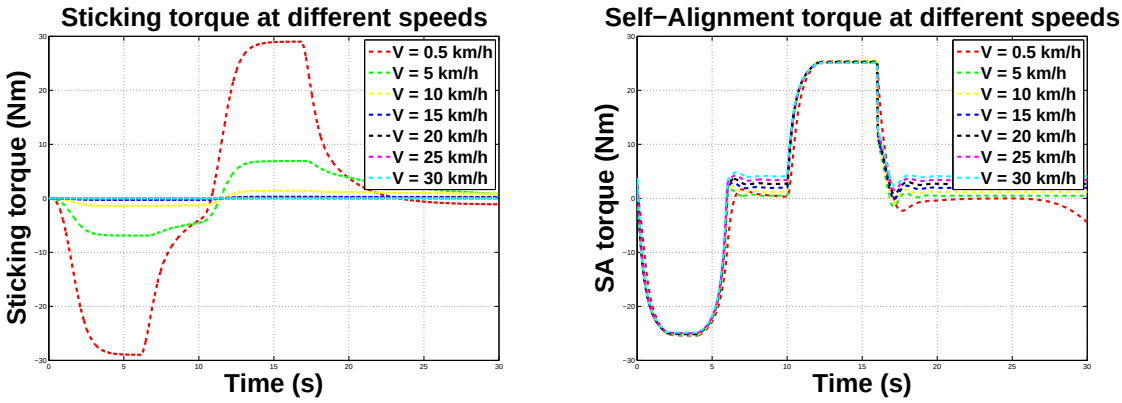


(a) (b)

Figure 10: Sticking torque (a) and Self-Alignment (b) torque for different driving speeds

# 4 Conclusions

This document presented simulation results of a detailed model of an EPS system including a dynamic model that reproduces the physical phenomena involved in driving. From an adequate mechanical model of the steering column, the natural oscillations that exist were eliminated. Furthermore, a satisfactory estimator of the exogenous torques was developed. Next, a dynamic friction model based on the LuGre model was successfully implemented in the simulation obtaining physically logical results.

# A Appendix

## A.1 Constants of the LuGre model

To evaluate the constants $\kappa_i^{ss}$ (for $i = x, y$)in Eq. (31) and $v^{ss}$ in Eq. (32), we have to know following steady-state equations of the system:

$$\begin{aligned}
\bar{z}_i^{ss} &= \frac{1}{F_n}\int_0^L z_i^{ss}(\zeta) f_n(\zeta) d\zeta = \\
&= \frac{1}{F_n}\Big[\frac{C_{1y}\alpha_1 {\zeta_L}^2}{2} - C_{1y}\alpha_1\left({C_{2y}}^2 - C_{2y}\left(C_{2y}+\zeta_L\right)e^{-\frac{\zeta_L}{C_{2y}}}\right) + \\
&- C_{1y} f_{max}\left(\zeta_L - \zeta_R + C_{2y}(e^{-\frac{\zeta_L}{C_{2y}}} - e^{-\frac{\zeta_R}{C_{2y}}})\right) \\
&+ C_{1y}\alpha_2\left(C_{2y}\left(C_{2y}+L\right)e^{-\frac{L}{C_{2y}}} - C_{2y}\left(C_{2y}+\zeta_R\right)e^{-\frac{\zeta_R}{C_{2y}}}\right) + \\
&+ C_{1y}\beta_2\left(L-\zeta_R\right) + \frac{C_{1y}\alpha_2}{2}(L^2 - {\zeta_R}^2) + C_{1y}C_{2y}\beta_2\left(e^{-\frac{L}{C_{2y}}} - e^{-\frac{\zeta_R}{C_{2y}}}\right)\Big]
\end{aligned} \tag{39}$$

$$\hat{z}_y^{ss} = \frac{1}{2\sigma_{0y}}(\sigma_{0y}\bar{z}_y^{ss} + \sigma_2 v_{ry}) - \frac{M_z^{ss}}{F_n L\sigma_{0y}} - \frac{G\sigma_{2y}v_{ry}}{F_n L\sigma_{0y}} \tag{40}$$

$z_i^{ss}(\zeta)$ is the steady-state function of the distributed model:

$$z_i^{ss}(\zeta) = C_{1i}(1 - e^{-\frac{\zeta}{C_{2i}}}) \tag{41}$$

$f_n(\zeta)$ is the trapezoidal load distribution:

$$f_n(\zeta) = \begin{cases} \alpha_1\zeta, & \text{for } 0 \le \zeta \le \zeta_L \\ f_{max}, & \text{for } \zeta_L \le \zeta \le \zeta_R \\ \alpha_2\zeta + \beta_2, & \text{for } \zeta_R \le \zeta \le L \end{cases} \tag{42}$$

$G$ is the following function:

$$\begin{aligned}
G &= \int_0^L f_n(\zeta)\zeta d\zeta = \\
&= \frac{\alpha_1}{3}\zeta_L^3 + \frac{f_{max}}{2}(\zeta_R^3 - \zeta_L^3) + \frac{\alpha_2}{3}(L^3 - \zeta_R^3) + \frac{\beta_2}{2}(L^2 - \zeta_R^2)
\end{aligned} \tag{43}$$

assuming $f_n(\zeta)$ as in Eq. (42).

$M_z^{ss}$ is the steady-state auto-aligning moment of the distributed model:

$$
\begin{aligned}
\mathrm{M_z^{ss}} &= \int_0^{\mathrm{L}} \left(\sigma_{0y} \mathrm{z_y^{ss}}(\zeta) + \sigma_{2y} \mathrm{v_{ry}}\right) \mathrm{f_n}(\zeta) \left(\frac{\mathrm{L}}{2} - \zeta\right) \mathrm{d}\zeta = \\
&= \mathrm{C_{1y}}\, \alpha_1\, \sigma_{0y} \left(2\,{\mathrm{C_{2y}}}^3 - {\mathrm{C_{2y}}}^3 \left(\frac{2\,\zeta_\mathrm{L}}{\mathrm{C_{2y}}} + \frac{{\zeta_\mathrm{L}}^2}{{\mathrm{C_{2y}}}^2} + 2\right) \mathrm{e}^{-\frac{\zeta_\mathrm{L}}{\mathrm{C_{2y}}}}\right) - \frac{1}{3}\alpha_1 {\zeta_\mathrm{L}}^3 (\mathrm{C_{1y}}\sigma_{0y} + \sigma_{2y}\,\mathrm{v_{ry}}) + \\
&- \frac{1}{2}\mathrm{C_{1y}}\ \mathrm{C_{2y}}, L\,\alpha_1\,\sigma_{0y} \left(\mathrm{C_{2y}} - \left(\mathrm{C_{2y}} + \zeta_\mathrm{L}\right) \mathrm{e}^{-\frac{\zeta_\mathrm{L}}{\mathrm{C_{2y}}}}\right) + \frac{L\,\alpha_1}{4} (\mathrm{C_{1y}}\sigma_{0y} {\zeta_\mathrm{L}}^2 + \mathrm{v_{ry}}\sigma_{2y} {\zeta_\mathrm{L}}^2) + \\
&+ \mathrm{C_{1y}}\, \mathrm{f_{max}}\, \sigma_{0y} \left(\mathrm{C_{2y}} \left(\mathrm{C_{2y}} + \zeta_\mathrm{L}\right) \mathrm{e}^{-\frac{\zeta_\mathrm{L}}{\mathrm{C_{2y}}}} - \mathrm{C_{2y}} \left(\mathrm{C_{2y}} + \zeta_\mathrm{R}\right) \mathrm{e}^{-\frac{\zeta_\mathrm{R}}{\mathrm{C_{2y}}}}\right) + \\
&+ \frac{\mathrm{C_{1y}}\, \mathrm{f_{max}}\, \sigma_{0y}}{2} ({\zeta_\mathrm{L}}^2 - {\zeta_\mathrm{R}}^2) + \frac{\mathrm{f_{max}}\, \sigma_{2y}\, \mathrm{v_{ry}}}{2} ({\zeta_\mathrm{L}}^2 - {\zeta_\mathrm{R}}^2) + \\
&- \frac{\mathrm{C_{1y}}\, L\, \mathrm{f_{max}}\, \sigma_{0y}}{2} (\zeta_\mathrm{L} + \zeta_\mathrm{R}) - \frac{L\, \mathrm{f_{max}}\, \sigma_{2y}\, \mathrm{v_{ry}}}{2} (\zeta_\mathrm{L} - \zeta_\mathrm{R}) + \\
&- \frac{1}{2}\mathrm{C_{1y}}\, \mathrm{C_{2y}}\, L\, \mathrm{f_{max}}\, \sigma_{0y} \left(\mathrm{e}^{-\frac{\zeta_\mathrm{L}}{\mathrm{C_{2y}}}} - \mathrm{e}^{-\frac{\zeta_\mathrm{R}}{\mathrm{C_{2y}}}}\right) + \frac{\mathrm{C_{1y}}\, \alpha_2\, \sigma_{0y}\, {\zeta_\mathrm{R}}^3}{3} + \\
&- \frac{\mathrm{C_{1y}}\, L^3\, \alpha_2\, \sigma_{0y}}{12} + \frac{\mathrm{C_{1y}}\, \beta_2\, \sigma_{0y}\, {\zeta_\mathrm{R}}^2}{2} - \frac{L^3\, \alpha_2\, \sigma_{2y}\, \mathrm{v_{ry}}}{12} + \\
&- \mathrm{C_{1y}}\, \alpha_2\, \sigma_{0y} \left({\mathrm{C_{2y}}}^3 \left(\frac{2\,L}{\mathrm{C_{2y}}} + \frac{L^2}{{\mathrm{C_{2y}}}^2} + 2\right) \mathrm{e}^{-\frac{L}{\mathrm{C_{2y}}}} - {\mathrm{C_{2y}}}^3 \left(\frac{2\,\zeta_\mathrm{R}}{\mathrm{C_{2y}}} + \frac{{\zeta_\mathrm{R}}^2}{{\mathrm{C_{2y}}}^2} + 2\right) \mathrm{e}^{-\frac{\zeta_\mathrm{R}}{\mathrm{C_{2y}}}}\right) + \\
&+ \sigma_{2y} \mathrm{v_{ry}} {\zeta_\mathrm{R}}^2 \left(\frac{\alpha_2}{3}\zeta_\mathrm{R} + \frac{\beta_2}{2}\right) - \mathrm{C_{1y}}\, \beta_2\, \sigma_{0y} \left(\mathrm{C_{2y}} \left(\mathrm{C_{2y}} + L\right) \mathrm{e}^{-\frac{L}{\mathrm{C_{2y}}}} - \mathrm{C_{2y}} \left(\mathrm{C_{2y}} + \zeta_\mathrm{R}\right) \mathrm{e}^{-\frac{\zeta_\mathrm{R}}{\mathrm{C_{2y}}}}\right) + \\
&+ \frac{1}{2}\mathrm{C_{1y}}\, L\, \alpha_2\, \sigma_{0y} \left(\mathrm{C_{2y}} \left(\mathrm{C_{2y}} + L\right) \mathrm{e}^{-\frac{L}{\mathrm{C_{2y}}}} - \mathrm{C_{2y}} \left(\mathrm{C_{2y}} + \zeta_\mathrm{R}\right) \mathrm{e}^{-\frac{\zeta_\mathrm{R}}{\mathrm{C_{2y}}}}\right) + \\
&- \frac{\mathrm{C_{1y}}\, L\, \beta_2\, \sigma_{0y}\, \zeta_\mathrm{R}}{2} - \frac{L\, \beta_2\, \sigma_{2y}\, \mathrm{v_{ry}}\, \zeta_\mathrm{R}}{2} - \frac{\mathrm{C_{1y}}\, L\, \alpha_2\, \sigma_{0y}\, {\zeta_\mathrm{R}}^2}{4} - \frac{L\, \alpha_2\, \sigma_{2y}\, \mathrm{v_{ry}}\, {\zeta_\mathrm{R}}^2}{4} + \\
&+ \frac{1}{2}\mathrm{C_{1y}}\, \mathrm{C_{2y}}\, L\, \beta_2\, \sigma_{0y} \left(\mathrm{e}^{-\frac{L}{\mathrm{C_{2y}}}} - \mathrm{e}^{-\frac{\zeta_\mathrm{R}}{\mathrm{C_{2y}}}}\right)
\end{aligned}
\tag{44}
$$

## References


[1] J. Illàn, V. Ciarla, and C. Canudas de Wit, *Oscillation annealing and driver/tire load torque estimation in electric power steering systems*, in Control Applications (CCA), 2011 IEEE International Conference on, pp. 1100âĂŞ1105, Sept. 2011.

[2] C. Canudas de Wit, S. Guégan, and A. Richard "*Control design for an electro power steering system: part I The reference model*", ECCÂŠ2001, European Control Conference, Porto(Portugal), septembre 2001 (invited)

[3] C. Canudas de Wit, S. Guégan, and A. Richard "*Control design for an electro power steering system: part II The control design*", ECCÂŠ2001, European Control Conference, Porto(Portugal), septembre 2001 (invited)

[4] E. Velenis, P. Tsiotras, C. Canudas de Wit and M. Sorine "*Dynamic Tire Friction Models for Combined Longitudinal and Lateral Vehicle Motion*", Vehicle System Dynamics, Volume 43, Issue 1 January 2005

[5] C. Canudas de Wit, P. Tsiotras, E. Velenis, M. Basset, and G. Gissinger, "*Dynamic friction models for road/tire longitudinal interaction*", Vehicle System Dynamics, vol. 39, no. 3, pp. 189 to 226, 2003